Extended Abstracts of the 2018 International Conference on Solid State Devices and Materials, Tokyo, 2018, pp675-676

Super-Nernstian Sensitivity of $CeTi_xO_y$ Sensing Film for pH Detection in Biofluid

Yu-Cheng Chou[1], Jim-Long Her[2], and Keiichi Koyama[3], and Tung-Ming Pan[1]*

[1]Department of Electronic Engineering, Chang Gung University, Taoyuan 333, Taiwan
[2]Division of Natural Science, Center for General Education, Chang Gung University, Taoyuan 333, Taiwan
[3]Graduate School of Science and Engineering, Kagoshima University, Kagoshima 890-0065, Japan
*Tel: +886-3-211-8800 ext. 3349, Fax:+886-3-211-8507, Email:tmpan@mail.cgu.edu.tw

Abstract

In this study, we proposed a microfabricated electrolyte–insulator–semiconductor (EIS) sensor based on $CeTi_xO_y$ sensing membrane for pH detection in biofluid. We attribute the super-Nernstian pH-sensitivity to surface phenomena at ion exchanging surface sites and redox transition between two oxidation states Ce^{3+} oxide and Ce^{4+} oxide.

1. Introduction

The pH monitoring and controlling are important part in nearly all processes involving water. The pH level of biofluids in all human beings is controlled by internal mechanism and maintained at certain range between 7.35 and 7.45. Beyond this range could demonstrate fatal [1]. Ceria-based material is famous for its redox property due to the reversible transformation from Ce^{4+} to Ce^{3+} valence states under oxidation-reduction process. However, the main problem when using CeO_2 films as sensing membranes is suffering from hygroscopicity due to its reaction with water, which degrades κ value. To overcome this issue, several researchers in literatures [2–4] have showed that the moisture absorption of the CeO_2 is suppressed by the incorporation of other elements (e.g., Ti, TiO_x, Y) into CeO_2 film.

2. Device Fabrication

The ~120 nm-thick $CeTi_xO_y$ sensing thin films were deposited on a p-type Si(100) substrate by reactive rf-magnetron co-sputtering using CeO_2 and metallic Ti targets. Rapid thermal annealing (RTA) was performed in oxygen ambient at different temperatures (700-900 ℃) for 30 s to improve the oxide quality. To define the sensing area of the deposited $CeTi_xO_y$, an automatic robotic dispenser was employed with an adhesive silicone gel acting as an isolating layer. The EIS sensor was assembled on a Cu wire on a custom-made PCB by silver glue.

3. Results and Discussion

In Fig. 1, we demonstrated the XRD patterns of $CeTi_xO_y$ sensing films annealed at various temperatures. A strong Ce_2O_3 (002) peak, and three weak $Ce_2Ti_2O_7$ (020), Ti_2O_3 (440) and (622) peaks appeared in the patterns of the samples annealed at 700 and 800 ℃. For the 900℃-annealed film, a strong CeO_2 (111) and three weak CeO_2 (200), (220) and (311) peaks were found.

Figs. 2(a)-(c) show the relative atomic concentrations (electron energy loss spectroscopy, EELS) of Ce, Ti, O, and Si as a function of relative position for the $CeTi_xO_y$ samples annealed at different temperatures. The sample after RTA at 700 and 800 ℃, relatively very small amount of Si with stable ~20 at% Ce, ~10 at% Ti and ~70 at% O were found in the bulk of the sample. The results further reveal that $CeTi_xO_y$ can be considered homogeneous in terms of elemental (Ce, Ti, and O) composition within the bulk of the sample.

The core level Ce 3d, Ti 2p, and O 1s XPS spectra with their appropriate peak curve-fitting lines for the $CeTi_xO_y$ sensing films annealed at different temperatures are shown in Fig. 3(a)-(c). As shown in Fig. 3(a), the Ce 3d spectra can be deconvoluted into three chemical compositions: v (~883.2 eV), v' (~885.4 eV) and v'' (~889.7 eV). The high binding energy peak (v'') and low binding energy (v) located at about 889.7 and 883.2 eV, respectively, are the result of a Ce^{4+} final state (CeO_2). The median binding energy state (v') located at ~885.4 eV is the result of a Ce^{3+} final state (Ce_2O_3). The area under v' peak corresponding to Ce^{3+} state and v'' peak corresponding to Ce^{4+} state gradually increases with RTA, which can be attributed to the valency shift of the Ce oxide. Additionally, the Ti 2p line at different RTA conditions in Fig. 3(b) suffers a shift of ~ 0.7 eV, relative to the TiO_2 reference position at 458.2 eV [5]. The positions of the Ti $2p_{1/2}$ and $2p_{3/2}$ peaks shifted to higher binding energies upon increasing the annealing temperature. Fig. 3(c) showed that the O 1s line spectra consist of three different peaks at 529.4, 530.3, and 531.5 eV can be correlated to the CeO_2, Ce_2O_3, and defective $CeTi_xO_y$ [6], respectively. The O 1s peak intensities provided by CeO_2 and Ce_2O_3 gradually increase upon increasing the RTA temperature, but suddenly decreased at 900 ℃. Fig. 4 shows that the surface roughness (R_{rms}) values of 1.70, 2.12 and 6.38 nm were determined for the $CeTi_xO_y$ films annealed at 700, 800 and 900 ℃, respectively. It can be found that the surface roughness value increased as the annealing temperature increased.

Figs. 5(a)–(c) demonstrate that the normalized C-V curves of $CeTi_xO_y$ EIS sensors annealed at various RTA temperatures shifted towards more negative voltage with increasing pH level. The insets to Figs. 5 (a)–(c) show the V_{REF} as function of pH values for the $CeTi_xO_y$ EIS devices after annealing at various temperatures. The pH-sensitivities of the $CeTi_xO_y$ films after RTA at 700, 800 and 900 ℃ were evaluated to be 70.86, 89.81 and 89.81 mV/pH, respectively. The $CeTi_xO_y$ EIS device annealed at both 800 and 900 ℃ exhibited the highest sensitivity. The higher surface roughness of the sensing membrane will give higher sensing performance. Higher surface roughness increases effectively the total surface area at oxide/electrolyte interface. On the other hand, Ce is an exception because of the stability of the empty f-shell in Ce^{4+}, where the nuclear charge is still low enough to allow the removal of the fourth valence electron [7]. From the XPS results, Ce element takes part in different redox activities. The incorporation of Ti element enhances the redox activity. As a result, only two electrons are transferred for every three protons, which the maximum slope for a Nernst

equation is as high as 88.5 mV/pH. Fig. 6 depicts (a) the hysteresis voltages of $CeTi_xO_y$ EIS devices annealed at various temperatures. The EIS sensor annealed at 800 ℃ exhibited the smallest hysteresis voltage (~1 mV), while that annealed at 900 ℃ had the highest (58 mV). Fig. 6(b) shows the drift characteristics of the $CeTi_xO_y$ EIS sensors annealed at the various RTA temperatures. The $CeTi_xO_y$ EIS sensor annealed at 800 ℃ exhibited the best long-term stability (0.34 mV/h), while the sensor annealed at 900 ℃ featured a serious drift rate (0.66 mV/h).

3. Conclusions

We presented a super-Nernstian response to pH from EIS sensors incorporating $CeTi_xO_y$ sensing films deposited through reactive co-sputtering. XRD, EELS, XPS, and AFM confirmed the well fabrication of $CeTi_xO_y$ sensing membrane in these EIS sensors. The pH-sensing performance of the CeT_xO_y EIS device annealed at 800 ℃ was superior to those of the devices subjected to other annealing temperatures, including a higher sensitivity of 89.81 mV/pH, a smaller hysteresis voltage of ~1 mV and a lower drift rate of 0.34 mV/h. This enhanced performance resulted from the formation of a stoichiometric $CeTi_xO_y$ film, a high surface roughness, and a low number of crystal defects.

Acknowledgment

The authors would like to thank the Ministry of Science and Technology of Taiwan for financially supporting this research under contract of MOST-106-2111-E-182-063.

References

[1] M. S. Cook, The Ultimate pH solution: Balance your body chemistry to prevent disease and lose weight; HarperCollins Publishers, New York, 2007.
[2] T. Schroeder et al., Appl. Phys. Lett. 87 (2005) 022902.
[3] R. B. van Dover, Appl. Phys. Lett. 74 (1999) 3041.
[4] Y. Zhao et al., Appl. Phys. Lett. 89 (2006) 252905.
[5] R. P. Netterfield et al., J. Appl. Phys. 66 (1989) 1805.
[6] V. Stetsovych et al., J. Phys. Chem. Lett. 4 (2013) 866.
[7] T. Yokota et al., Appl. Phys. Lett. 81 (2002) 4023.

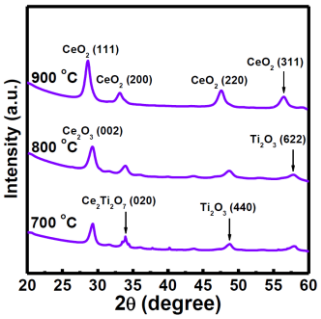

Fig. 1. XRD patterns of $CeTi_xO_y$ films annealed at various temperatures.

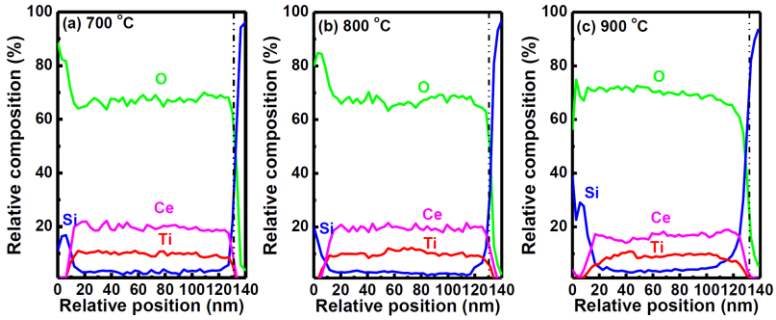

Fig. 2. Relative atomic concentrations of Ce, Ti, O, and Si as a function of relative position for CeT_xO_y sensing films annealed at (a) 700, (b) 800 and (c) 900 ℃.

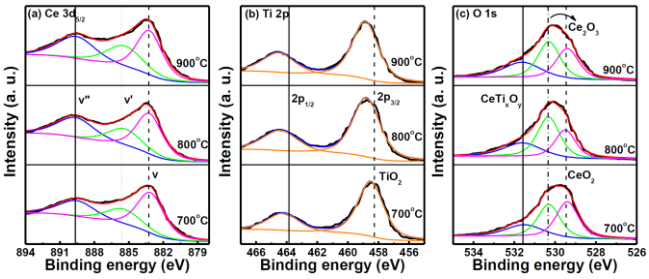

Fig. 3. XPS spectra displaying the (a) Ce 3d, (b) Ti 2p, and (c) O 1s energy levels in $CeTi_xO_y$ films annealed at various temperatures.

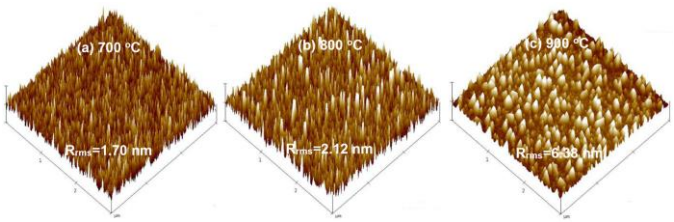

Fig. 4. AFM images of $CeTi_xO_y$ films sensing films annealed at (a) 700, (b) 800 and (c) 900 ℃.

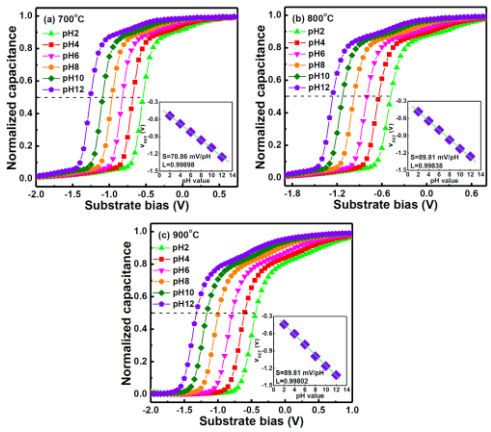

Fig. 5. Responses of the *C–V* curves for $CeTi_xO_y$ EIS sensors annealed at (a) 700, (b) 800 and (c) 900 ℃. Insets: Reference voltages plotted with respect to pH for the $CeTi_xO_y$ EIS sensors.

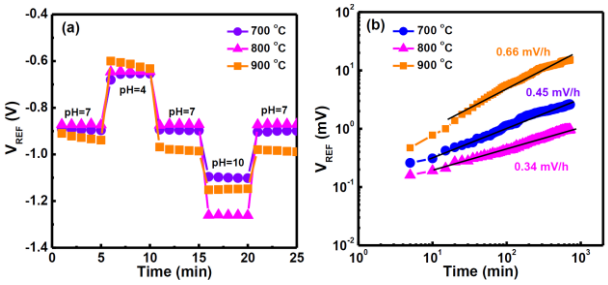

Fig. 6. (a)Hysteresis curves and (b) drift rates of $CeTi_xO_y$ EIS sensors annealed at various temperatures measured in pH 7→4→7→10→7 and pH 7, respectively.